International Journal of Biological Macromolecules 151 (2020) 976–983

Contents lists available at ScienceDirect

International Journal of Biological Macromolecules

journal homepage: http://www.elsevier.com/locate/ijbiomac

Improved performances of catalytic G-quadruplexes (G4-DNAzymes) *via* the chemical modifications of the DNA backbone to provide G-quadruplexes with double 3′-external G-quartets

Antonella Virgilio [a,1], Veronica Esposito [a,1], Pauline Lejault [b], David Monchaud [b,*], Aldo Galeone [a,*]

[a] Department of Pharmacy, University of Naples Federico II, Napoli, Italy
[b] ICMUB CNRS UMR6302, UBFC Dijon, 9, Avenue Alain Savary, Dijon 21078, France

ARTICLE INFO

Article history:
Received 31 August 2019
Received in revised form 18 October 2019
Accepted 22 October 2019
Available online 17 November 2019

Keywords:
DNAzyme
Tetramolecular G-quadruplex
Peroxidase activity
Hemin

ABSTRACT

Here we report on the design of a new catalytic G-quadruplex-DNA system (G4-DNAzyme) based on the modification of the DNA scaffold to provide the DNA pre-catalyst with two identical 3′-ends, known to be more catalytically proficient than the 5′-ends. To this end, we introduced a 5′-5′ inversion of polarity site in the middle of the G4-forming sequences AG_4A and AG_6A to obtain d($^{3'}$AGG$^{5'}$-$^{5'}$GGA$^{3'}$) (or AG_2-G_2A) and d($^{3'}$AGGG$^{5'}$-$^{5'}$GGGA$^{3'}$) (or AG_3-G_3A) that fold into stable G4 whose tetramolecular nature was confirmed *via* nuclear magnetic resonance (NMR) and circular dichroism (CD) investigations. Both AG_2-G_2A and AG_3-G_3A display two identical external G-quartets (3′-ends) known to interact with the cofactor hemin with a high efficiency, making the resulting complex competent to perform hemoprotein-like catalysis (G4-DNAzyme). A systematic comparison of the performances of modified and unmodified G4s lends credence to the relevance of the modification exploited here (5′-5′ inversion of polarity site), which represents a new chemical opportunity to improve the overall activity of catalytic G4s.

1. Introduction

The catalytic activity of quadruplex-DNA (G4), often referred to as quadruplex DNAzyme or G4-DNAzyme, was discovered as an aftermath of investigations aiming at identifying aptamers prone to catalyze porphyrin metalation [1]. Given that N-methylmesoporphyrin IX (NMM) is a known transition-state analogue for porphyrin metalation, Sen et al. searched for aptamers with a high NMM affinity [2]. Systematic evolution of ligands by exponential enrichment (SELEX) experiments lead to the identification of a 24-nt DNA named PS5.M that binds NMM with exquisite affinity. As expected, PS5.M catalyses the metalation of mesoporphyrin IX but it was also discovered that this catalytic activity is inhibited by protoporphyrin IX iron(III) chloride, or hemin (Fig. 1), owing to the formation of a high-stability PS5.M/hemin complex. Given that hemin is a known cofactor of many enzymes (heme-dependent enzymes, or hemoenzymes), the hemoprotein-like properties of PS5.M were investigated: like peroxidases, the presence of a stoichiometric oxidant (hydrogen peroxide, H_2O_2), was found to strongly increase the PS5.M/hemin complex-mediated oxidation rate of a model substrate, the chromogenic ABTS (Fig. 1), or 2,2′-azino-bis (3-ethylbenzothiazoline-6-sulfonic acid [3]. These results provided the proof-of-concept that nucleic acids can perform oxidase-type catalysis. The G4-DNAzyme nature of this novel system was demonstrated later on: both the nature of the sequence of PS5.M d($^{5'}$GTG$_3$TCAT$_2$GTG$_3$TG$_3$TGTG$_2^{3'}$) and the dependence of its catalytic activity upon K^+-rich buffers were indeed strongly suggestive of a G4 pre-catalyst [4]. The hypothesis, which is now widely accepted, was that G4 offers a binding site to hemin, which becomes catalytically proficient only upon interaction with the external G-quartet of the DNA pre-catalyst (Fig. 1). It is intriguing that, more than three decades after its discovery, the exact mechanism of G4-DNAzyme is still unclear and debated [5–8]. Despite this, dozens of new G4-DNAzymes are reported yearly [9–12] with multiple biosensing applications [13,14] ranging from metal detection [15–18] to mRNA detection [19,20], now resolutely pointing towards industry-relevant applications.

Over the past years, various strategies have been devised to improve the overall catalytic efficiency of G4-DNAzymes and make them competitive with hemoproteins. The effects of the modification of the sequence and thus, of the structure of the G4 pre-catalysts have been studied [21,22], along with those of external G-quartet flanking nucleotides [23–25]. The addition of external boosting agents has also been studied (such as adenine triphosphate (ATP) [5,26], template-assembled synthetic G-quartet (TASQ) [27] or spermine [28]), as well

* Corresponding authors.
E-mail addresses: david.monchaud@cnrs.fr (D. Monchaud), galeone@unina.it (A. Galeone).
[1] These authors contributed equally.

https://doi.org/10.1016/j.ijbiomac.2019.10.181
0141-8130/

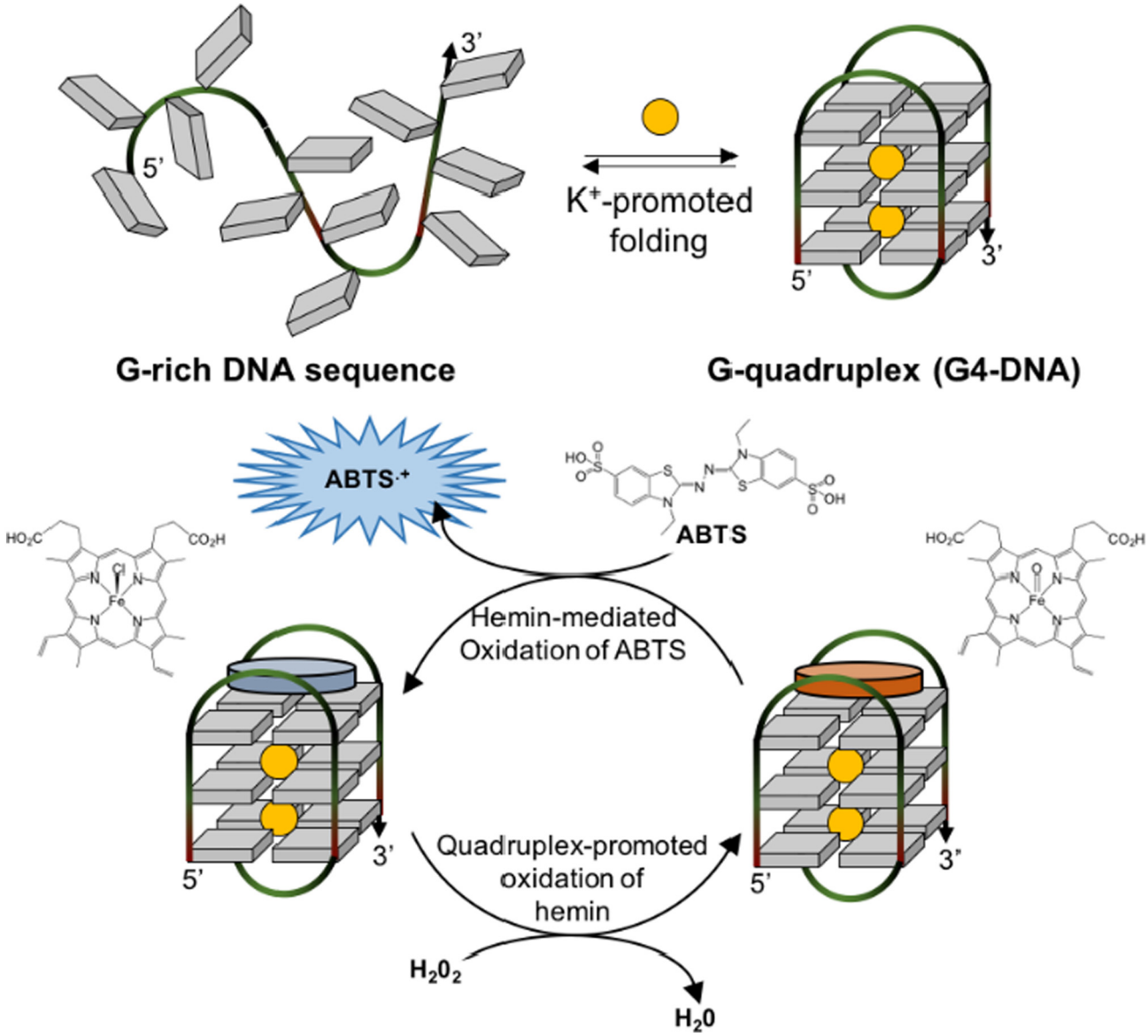

Fig 1. Schematic representation of the folding of a guanine (G)-rich DNA sequence into a G-quadruplex-DNA (G4-DNA, upper panel), and of a G4-DNAzyme catalysis, here the H_2O_2-promoted oxidation of ABTS.

as the conjugation of ligand-binding aptamer (i.e., the 'nucleoapzyme' approach [29]). The role of the temperature was also investigated: DNAzymes with better catalytic performances at elevated temperatures were uncovered (so called thermophilic G4-DNAzymes) [30], on the basis of highly thermally stable tetramolecular G4 pre-catalysts. This approach is interesting in that it tackles one pitfalls usually associated with nucleic acid catalysts, i.e., their supposed sensitivity to harsh experimental conditions. Here, we report on a brand new approach aiming at using G4 pre-catalysts with two identical external G-quartets. Indeed, in all studies reported so far, G4s display different external quartets (so called 5′- and 3′-quartets, or 5′- and 3′-ends) while it has been demonstrated that the 3′-end is more catalytically competent than its 5′-counterpart [7]. We thus decide to design and synthesize G4s with two external 3′-ends according to an original approach based on the introduction of a 5′-5′ inversion of polarity site in the middle of the G4-forming strands d($^{5'}$AGGGGA$^{3'}$) (or AG_4A) and d($^{5'}$AGGGGGGA$^{3'}$) (or AG_6A), known to form an efficient G4-DNAzyme system. The catalytic dividend of this approach is three-fold: *i*- the major role of the 3′-end in binding hemin, critical to promote the catalytic process efficiently; *ii*- the high thermal stability of a tetramolecular quadruplex with inverted polarity, as already demonstrated with d($^{3'}$TGG$^{5'}$-$^{5'}$GGT$^{3'}$) (or TG_2-G_2T) [31], to use them as thermophilic pre-catalysts; and *iii*- the beneficial presence of adenines (dA) on the 3′-end, which help hemin stacking and thus, the catalysis [7]. We thus report here on the synthesis of the 6- and 8-nt sequences d($^{3'}$AGG$^{5'}$-$^{5'}$GGA$^{3'}$) (or AG_2-G_2A) and d($^{3'}$AGGG$^{5'}$-$^{5'}$GGGA$^{3'}$) (or AG_3-G_3A) that fold into G4s with two adenine-capped 3′-ends (Fig. 2), whose high thermal stability allows for their use as thermophilic DNAzyme pre-catalysts.

2. Materials and methods

2.1. Oligonucleotide synthesis and purification

The modified oligonucleotides (ODNs) and their natural counterparts were synthesized on a Millipore Cyclone Plus DNA synthesizer using solid phase β-cyanoethyl phosphoramidite chemistry at 15 μmol scale. The synthesis of the 3′-5′ tracts were performed by using normal 3′-phosphoramidites, whereas the 5′-3′ tracts were synthesized by using 5′-phosphoramidites. For all ODNs an universal support was used. The oligomers were detached from the support and deprotected

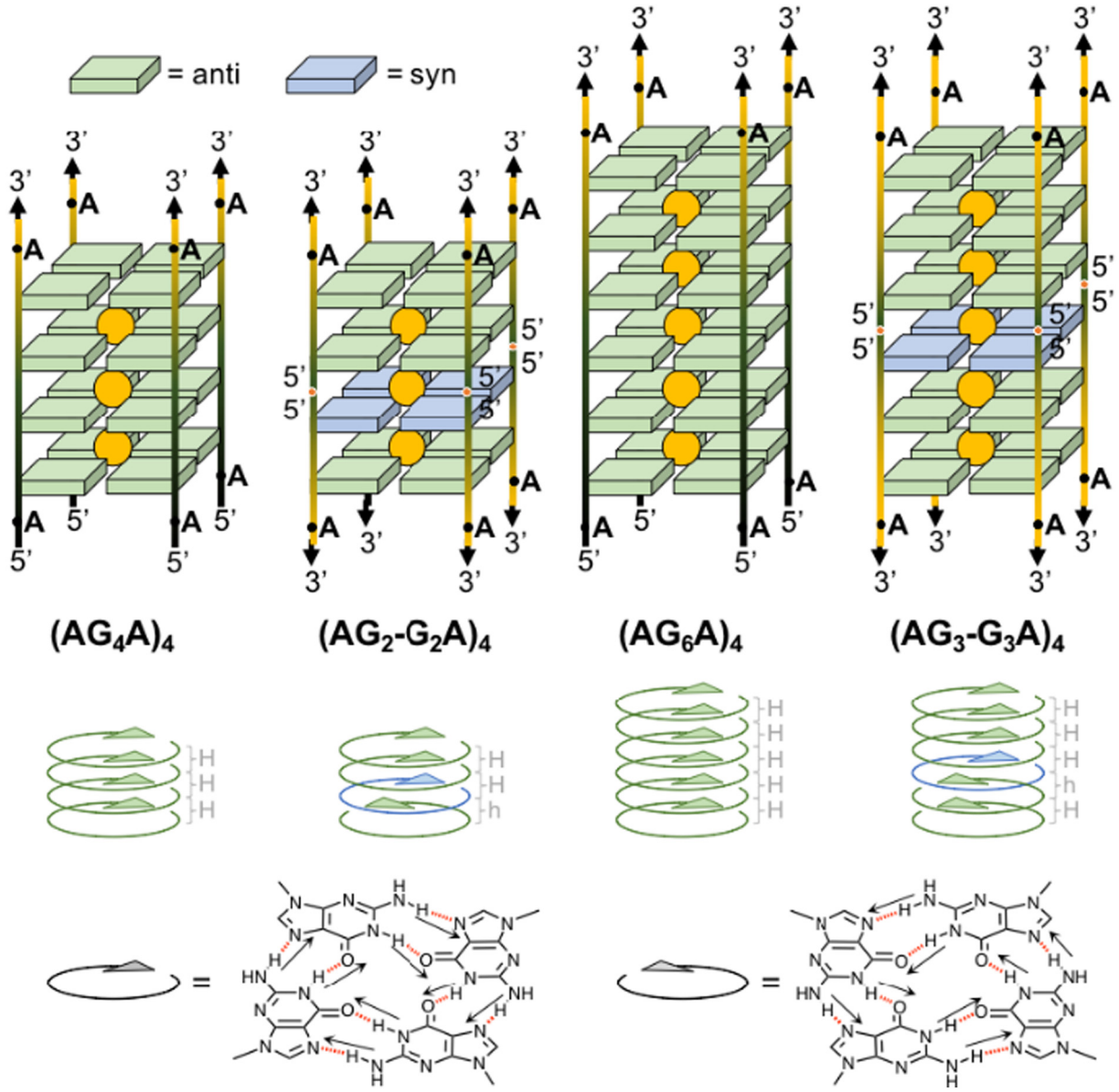

Fig. 2. Schematic representation of the G-quadruplex structures formed by AG_4A, AG_2-G_2A, AG_6A and AG_3-G_3A. Anti and syn residues are in green and blue, respectively. Details about the H-bond directionality of G-quartets; "H" and "h" for homopolar and heteropolar stacking, respectively.

by treatment with concentrated aqueous ammonia at 80 °C overnight. The combined filtrates and washings were concentrated under reduced pressure, redissolved in H_2O, analyzed and purified by high-performance liquid chromatography on a Nucleogel SAX column (Macherey–Nagel, 1000-8/46), using buffer A: 20 mM NaH_2PO_4/Na_2HPO_4 aqueous solution (pH 7.0) containing 20% (v/v) CH_3CN and buffer B: 1 M NaCl, 20 mM NaH_2PO_4/Na_2HPO_4 aqueous solution (pH 7.0) containing 20% (v/v) CH_3CN; a linear gradient from 0 to 100% B for 30 min and flow rate 1 mL/min were used. The fractions of the oligomers were collected and successively desalted by Sep-pak cartridges (C-18). The isolated oligomers proved to be 95% pure by NMR.

2.2. NMR spectroscopy

NMR samples were prepared at a concentration of about 2.0 mM, in 0.6 mL (H_2O/D_2O 9:1 v/v) buffer solution having 10 mM KH_2PO_4/K_2HPO_4, 40 mM KCl and 0.2 mM EDTA (pH 7.0). All the samples were heated for 5–10 min at 90 °C and slowly cooled (10–12 h) to room temperature. The solutions were equilibrated for several weeks at 4 °C. The annealing process was assumed to be complete when ^{1}H NMR spectra were superimposeable on changing time. NMR spectra were recorded with Varian Unity INOVA 500 MHz spectrometer. 1D proton spectra of the sample in H_2O were recorded using pulsed-field gradient DPFGSE for H_2O suppression. ^{1}H-chemical shifts were referenced relative to external sodium 2,2-dimethyl-2-silapentane-5-sulfonate (DSS). Pulsed-field gradient DPFGSE sequence was used for NOESY (180 ms and 80 ms mixing times) and TOCSY (120 ms mixing time) experiments in H_2O. All experiments were recorded using STATES-TPPI procedure for quadrature detection. In all 2D experiments, the time domain data consisted of 2048 complex points in t2 and 400–512 fids in t1 dimension. A relaxation delay of 1.2 s was used for all experiments.

2.3. CD spectroscopy

CD samples of modified oligonucleotides and their natural counterpart were prepared from stock solutions annealed under the same conditions as NMR and diluted just before the acquisition at a ODN concentration of 70 μM by using a buffer solution 10 mM KH_2PO_4/

K_2HPO_4, 40 mM KCl (pH 7.0). CD spectra of all quadruplexes and CD melting curves were registered on a Jasco 715CD spectrophotometer. For the CD spectra, the wavelength was varied from 220 to 320 nm at 100 nm min^{-1} scan rate, and the spectra recorded with a response of 16 s, at 2.0 nm bandwidth and normalized by subtraction of the background scan with buffer. The temperature was kept constant at 20 °C with a thermoelectrically-controlled cell holder (Jasco PTC-348). CD melting curves were registered as a function of temperature (range: 20 °C-95 °C) for all quadruplexes at their maximum Cotton effect wavelengths. The CD data were recorded in a 0.1 cm pathlength cuvette with a scan rate of 0.5 °C/min.

2.4. DNAzyme experiments

All chemicals were purchased from Sigma-Aldrich and used without purification (including hemin (iron(III) protoporphyrin chloride, from bovine) and ABTS (2,2′-Azino-bis (3-ethylbenzothiazoline-6-sulfonic acid)). The lyophilized DNA control strands (AG_4A and AG_6A) were purchased from Eurogentec, Seraing, Belgium and firstly diluted at 1000 μM in deionized water (18.2 MΩ.cm resistivity). All DNA structures were prepared in a Caco.K buffer, comprised of 10 mM lithium cacodylate buffer (pH 7.2) plus 40 mM KCl/60 mM LiCl. Quadruplex structures were prepared by mixing 100 μL of constitutive strand (1000 μM) with 20 μL of a lithium cacodylate buffer solution (100 mM, pH 7.2), plus 20 μL of a KCl/LiCl solution (400 mM/600 mM) and 60 μL of water. The final concentrations were theoretically 125 μM per motif G4.

The actual concentration of each DNA was determined through a dilution to 1 μM theoretical concentration through UV spectral analysis at 260 nm (after 5 min at 90 °C) with the following molar extinction coefficient values: AG_4A ($\varepsilon = 69000\ l\ mol^{-1}\ cm^{-1}$), AG_6A ($\varepsilon = 89200\ l\ mol^{-1}\ cm^{-1}$), AG_2-G_2A ($\varepsilon = 69000\ l\ mol^{-1}\ cm^{-1}$), AG_3-G_3A ($\varepsilon = 89200\ l\ mol^{-1}\ cm^{-1}$). The G4 DNA structures were folded by heated (90 °C, 5 min), gradually cooled (65, 60, 55, 50, 40 and 30 °C (30 min/step), 25 °C (2 h) and then stored at least two days at 4 °C.

2.4.1. Optimization of H_2O_2 concentration

All the experiments were carried out at 20 °C with Caco.KTD buffer, comprised of 10 mM lithium cacodylate buffer (pH 7.2) plus 40 mM KCl / 60 mM LiCl, 0.05% Triton X-100 and 0.1% DMSO. Stock solutions were ABTS (20 mM in water), hemin (100 μM in DMSO), H_2O_2 (100 mM in water) and tetramolecular G4 (125 μM per motif). Experimental conditions were defined as: ABTS (1 mM), hemin (1 μM), tetramolecular G4 (1 μM) and increasing amounts of stoichiometric oxidant H_2O_2 (from 0.2 to 1.0 mM). G4s and hemin mixtures in Caco.KTD buffer were stirred at room temperature for 30 min, then ABTS were added and the DNAzyme reactions were thus initialized by the addition of H_2O_2. The experiments were carried out in 1 mL-quartz cuvettes (Starna) on a JASCO V630Bio spectrophotometer with a thermally controlled six-cell holded.

2.4.2. Optimization of thermophilic DNAzyme

All the experiments were carried out with Caco.KTD buffer, comprised of 10 mM lithium cacodylate buffer (pH 7.2) plus 40 mM KCl / 60 mM LiCl, 0.05% Triton X-100 and 0.1% DMSO. Stock solutions were ABTS (20 mM in water), hemin (100 μM in DMSO), H_2O_2 (20 mM in water) and tetramolecular G4 (125 μM per motif). Experimental conditions were defined as: ABTS (2 mM), hemin (1 μM), tetramolecular G4 (1 μM) and 0.2 mM of H_2O_2. G4s and hemin mixtures in Caco.KTD buffer were stirred at room temperature for 30 min, then ABTS were added and the DNAzyme reactions were thus initialized by the addition of H_2O_2. The experiments were carried out in a 96-well plate on a Thermo Scientific Multiskan controlled by SkanIt software.

For all of experiments, the characteristic UV–Vis signal of ABTS at 420 nm (recorded every 60 s) was collected and plotted as a function of time with OriginPro® 2018 software. Raw data were firstly subtracted from the control experiment (carried out in the same conditions without G-quadruplex) and, for sake of comparison, subsequently zeroed at their very first point. The initial rates (V_0 in min^{-1}) were similarly determined by fitting as a linear function the 4 very first points.

3. Results and discussion

3.1. NMR spectroscopy

The ability of AG_2-G_2A and AG_3-G_3A to form G4s was investigated by NMR and CD spectroscopy. Both sequences AG_2-G_2A and AG_3-G_3A are characterized by symmetry planes through the phosphate groups that form the inversion of polarity sites joining the two halves (Fig. 2). The occurrence of imino proton resonances in the 10.5–12.0 ppm region in ^1H NMR spectra is a distinctive feature of G-tetrad formation. Therefore, the inspection of this region is commonly used to gain structural insights into the G4 structure, notably its symmetry. The ^1H NMR spectra of AG_2-G_2A and AG_3-G_3A collected at 25 °C in K^+ buffer (Fig. 3) show the presence of respectively 4 and 6 main signals (two of them overlap in both cases) in the region 10.5–12.0 ppm, attributable to imino protons involved in Hoogsteen hydrogen bonds of G-quartets. 8 and 10 other aromatic signals can be seen for AG_2-G_2A and AG_3-G_3A, respectively, which correspond to the H8 of dG (or G-H8) and to the H2/H8 of dA (A-H2 and A-H8). These sets of signals indicate that both G4s are formed but also that these structures are non-symmetrical, in contrast with their sequences. ^1H NMR spectra of AG_4A and AG_6A samples were acquired in the same conditions: the simple appearance of both ^1H NMR profiles indicates that the unmodified oligomers form mainly a single well-defined hydrogen-bonded conformation, showing the appropriate number of imino proton signals diagnostic of the presence of G-quadruplex structures (10.5–12.0 ppm) (Fig. S1).

To gain further structural insights into the G4-complexes formed by AG_2-G_2A and AG_3-G_3A, 2D NMR was implemented. Most of the ^1H NMR resonances were assigned by means of the analysis of 2D TOCSY (data not shown) and 2D NOESY experiments (Fig. S2 and S3, Table S1). Collected data indicate that both G4s adopt a parallel-like structure, in which the 5′-5′ inversion of polarity site of each strand is in the same position within the G4 structure. The 2D NOESY spectra indicate NOEs between G-H8 and A-H8 and their own H1′, H2′ and H2″ ribose protons and the H1′, H2′ and H2″ protons of the residue on the 5′-side, typical of parallel G-quadruplex structures. As expected, the path of NOE connectivities is broken at the 5′-5′ inversion of polarity site. The existence of NOE sequential connectivities along the two subunits of the strand suggests that the backbones adopt a helical winding. Regarding the glycosidic torsion angles, the presence of both weak NOEs between G-H8/A-H8 and the corresponding ribose H1′ and strong NOEs between G-H8/A-H8 and ribose H2′ indicates that most of guanosines possess *anti* glycosidic conformations (in green, Fig. 2). However, for both samples, one dG residue adjacent to the 5′-5′ inversion of polarity site was characterized by the presence of a strong NOE cross-peak involving G-H8 and H1′ ribose proton that indicates *syn* glycosidic conformations for these residues, as also confirmed by the characteristic downfield shift of their H2′ signals (Figs. S2, S3 and Table S1). Collectively, NMR data indicate that both G4s display a single all-*syn* G-tetrad, lying in the middle of the structure, adjacent to the 5′-5′ inversion of polarity site (in blue, Fig. 2), as already demonstrated in similar G4s [31,32]. In both cases, NOE contacts between H8 and H1′ of dGs flanking the 5′-5′ inversion of polarity site were observed, indicative of a spatial vicinity between the all-*anti* and all-*syn* G-tetrads. Interestingly, differently from AG_2-G_2A, AG_3-G_3A was characterized by interstrand NOEs between A-H8 and A-H2 of adjacent strand, suggesting that dA residues were not randomly oriented, being close to each other and oriented in a symmetrical fashion.

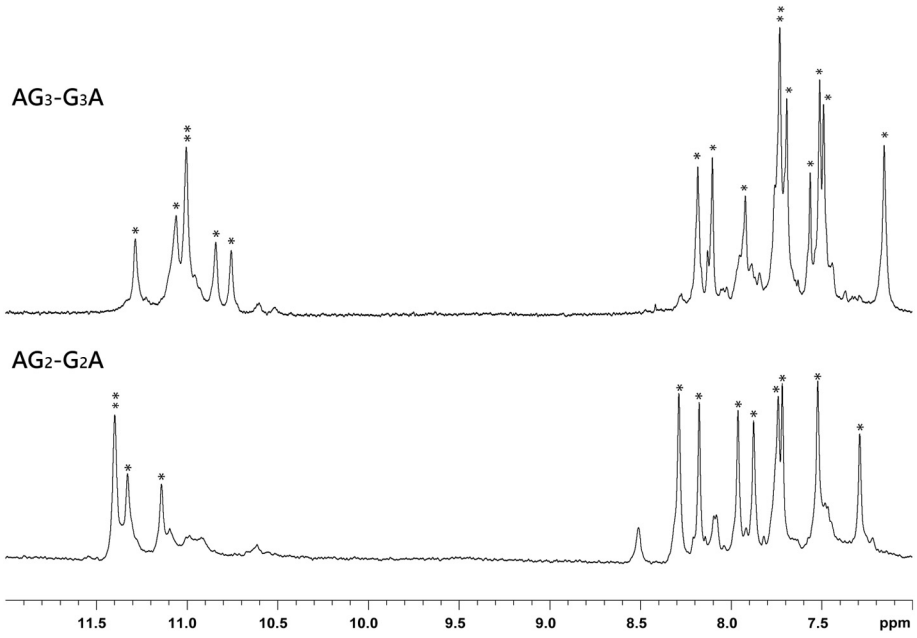

Fig. 3. Imino and aromatic proton regions of the G-quadruplex structures formed by the ODNs containing inversion of polarity sites. Stars indicate the signals of the main structures.

3.2. CD spectroscopy

To go a step further, CD spectra of both AG_2-G_2A and AG_3-G_3A, along with their unmodified counterparts AG_4A and AG_6A, were acquired at 20 °C (Fig. 4). All measurements were performed at a concentration of 70 μM oligonucleotide strand with a buffer containing 40 mM KCl. As previously reported [30], the unmodified G-quadruplexes AG_4A and AG_6A showed CD spectra with a maximum around 264 nm and a minimum around 240 nm, typical of tetramolecular parallel G4s with all-*anti* G-tetrads (schematically represented in Fig. 2) [33,34]. The CD profile of AG_2-G_2A was characterized by an unusual profile, with two positive bands of similar intensity, centred on 250 and 298 nm (Fig. 4A), in line with what was already described with TG_2-G_2T [31]. On the other hand, the CD profile of AG_3-G_3A was characterized by a major positive band at 263 nm and a minor positive one at 298 nm (Fig. 4B). These data can be explained taking into account the number and nature of stacked G-tetrads. Indeed, G-tetrads are characterized by a H-bond directionality: two stacked G-tetrads can thus be of similar or opposite directionality (homopolar (H) and heteropolar (h) stacking, respectively) [34] (Fig. 2). In the case of AG_2-G_2A the contribution of heteropolar stacking to the CD signal is not negligible (2H *versus* 1 h), thus resulting in the unusual CD profile observed. On the contrary, the homopolar stacking is dominant with AG_3-G_3A (4H *versus* 1 h), making the overall CD spectrum very similar to those of AG_4A and AG_6A, in which only homopolar stackings occur. Collectively, these results are in agreement with the strands orientation and tetrads arrangements provided by the NMR analysis (Fig. 3). Finally, CD-melting experiments were used to evaluate the thermal stability of this array of 4 G4s (Fig. S4): none of them melted at temperature <90 °C, thus demonstrating their very high thermal stability.

3.3. DNAzyme experiments

We decided to assess whether these G4s (both the modified AG_2-G_2A and AG_3-G_3A and the unmodified AG_4A and AG_6A) were catalytically competent. We first used the standard ABTS oxidation protocol [5] performed with a stoichiometric amount of DNA pre-catalyst and hemin (1 μM) in a presence of an excess of substrate (ABTS, 2 mM), the catalysis being triggered by the addition of H_2O_2 (0.2 mM). As seen in Fig. 5, the ABTS oxidation was efficient as monitored *via* the evolution of the absorbance of $ABTS^{\cdot+}$ at 420 nm as a function of time. Interestingly, AG_2-G_2A and AG_3-G_3A displayed a better activity (initial

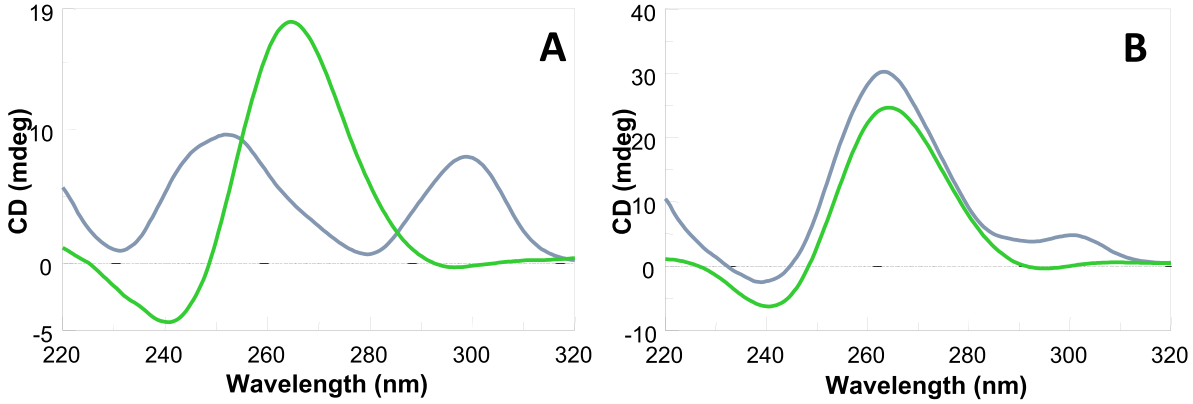

Fig. 4. CD profiles of (A) AG_4A (green) and AG_2-G_2A (blue); and (B) AG_6A (green) and AG_3-G_3A (blue) (70 μM, 40 mM K^+, 20 °C).

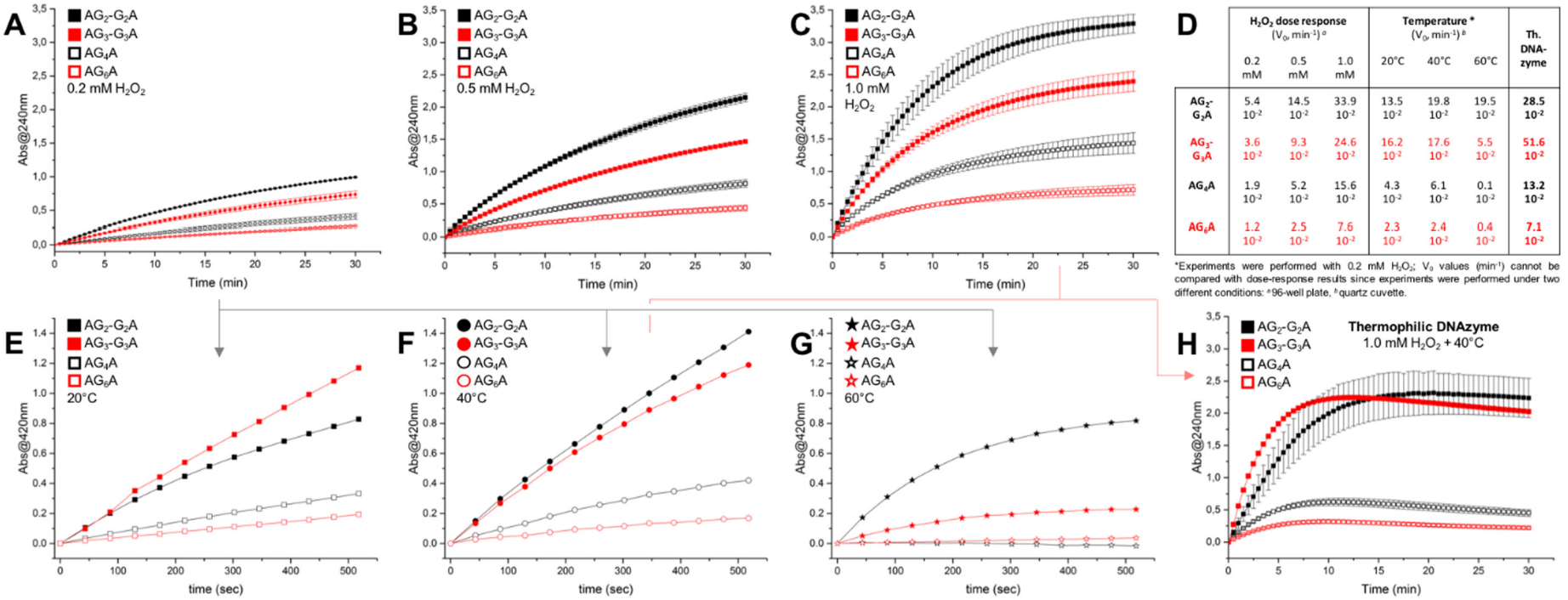

Fig. 5. DNAzyme results of experiments performed with 1 μM G4 (the modified AG_2-G_2A and AG_3-G_3A and their unmodified counterparts AG_4A and AG_6A), 1 μM hemin, 2 mM ABTS and increasing amounts of stoichiometric oxidant H_2O_2 (from 0.2 to 1.0 mM, A–C) at 20 °C, or with 0.2 mM H_2O_2 with increasing temperature (from 20 to 60 °C, E–G). Optimized thermophilic DNAzyme was designed with 1 μM G4, 1 μM hemin, 2 mM ABTS, 1.0 mM H_2O_2 at 40 °C (H). All experiments are performed in either 96-well plates (A–C, H) or quartz cuvettes (E–G). See Supporting Information for details. Initial velocity V_0 values (min^{-1}) are summarized in table D.

velocity $V_0 = 5.4$ and $3.6\ 10^{-2}\ min^{-1}$, respectively, Fig. 5D) than their unmodified counterparts (with $V_0 = 1.9$ and $1.2\ 10^{-2}\ min^{-1}$ for AG_4A and AG_6A, respectively, *i.e.*, ~3-fold less active). Expectedly, their catalytic competences were directly function of the H_2O_2 concentration (the more, the better, Fig. 5A-C), with V_0 up to 33.9 and $24.6\ 10^{-2}\ min^{-1}$ for AG_2-G_2A and AG_3-G_3A, respectively, still better than their unmodified counterparts (with V_0 up to 15.6 and $7.6\ 10^{-2}\ min^{-1}$ for AG_4A and AG_6A, respectively). These results, fully in line with the double 3′-ends of modified G4s, have to be compared to the performances of intramolecular G4s. For instance, 22AG d($^{5'}AG_3(T_2AG_3)_3^{3'}$), which was studied as a possible biologically relevant catalytic G4, displayed lower performances ($V_0 = 2.7\ 10^{-2}\ min^{-1}$) under comparable experimental conditions (1 μM DNA, 1 μM hemin, 2 mM ABTS and 0.6 mM H_2O_2) [35]. However, specially dedicated intramolecular G4 such as the series of G3T d($^{5'}G_3TG_3TG_3TG_3^{3'}$) derivatives developed by Zhou *et al.* were found more efficient, with V_0 up to $40.0\ 10^{-2}\ min^{-1}$ for lower catalyst loading (0.4 μM DNA, 0.8 μM hemin, 0.6 mM ABTS and 0.6 mM H_2O_2) [7]. However, these results cannot be directly compared to the tetramolecular G4 folded from the d($^{5'}AG_5A^{3'}$) used as thermophilic DNAzyme [30]: in these experiments, AG_5A was found highly efficient at room temperature (with $V_0 = 60.0\ 10^{-2}\ min^{-1}$) at a concentration of 0.86 μM DNA, upon addition of 1.72 μM hemin, 1.28 mM ABTS and 1.28 mM H_2O_2. We next decided to assess whether AG_2-G_2A and AG_3-G_3A might behave as thermophilic G4-DNAzyme, performing catalysis at 20, 40 and 60 °C (Fig. 5E-G) under our predefined conditions (*vide supra*). The catalytic proficiencies of these G4 systems increased with the temperature, to be optimal at 40 °C ($V_0 = 19.8$ and $17.6\ 10^{-2}\ min^{-1}$ for AG_2-G_2A and AG_3-G_3A, respectively, *versus* 6.1 and $2.4\ 10^{-2}\ min^{-1}$ for AG_4A and AG_6A, respectively). These results highlighted that a subtle equilibrium has to be reached when designing thermophilic DNAzymes, dealing with temperature-promoted catalysis, G4 thermal stability and efficient hemin binding that likely involves the wreath of adenine on the 3′-ends of the G4s. We finally decided to combine optimal H_2O_2 concentration (1.0 mM) and temperature (40 °C) to design new thermophilic DNAzymes made of G4s embedding 5′-5′ inversion of polarity site (Fig. 5H) that proved efficient ($V_0 = 28.5\ 10^{-2}\ min^{-1}$ for AG_2-G_2A) and very efficient ($V_0 = 51.6\ 10^{-2}\ min^{-1}$ for AG_3-G_3A), especially with regard to their unmodified counterparts ($V_0 = 13.2$ and $7.1\ 10^{-2}\ min^{-1}$ for AG_4A and AG_6A, respectively, i.e., up to 7-fold less active).

Overall, the systematic comparison of the performances of the modified AG_2-G_2A/AG_3-G_3A *versus* the unmodified AG_4A/AG_6A precatalysts clearly shows that the unmodified G4s are systematically less active than the modified G4s, whatever the experimental conditions they are used in (concentration, temperature, etc.). These results thus confirmed the relevance of our chemical modification approach, combining 5′-5′ inversion of polarity site and introduction of 3′-end dA caps, and provide a solid basis for designing ever more efficient DNA-based molecular devices.

4. Conclusions

The discovery of catalytic DNAs has spurred promising biotechnological developments thanks to the unique properties of nucleic acids in terms of chemical versatility and programmable functionalities [36]. Nucleic acids indeed have key advantages over protein enzymes (size, synthetic access, tunable sequences) but their catalytic properties do not still reach the performances of their proteinic counterparts. This lower catalytic proficiency might originate in less structurally defined active sites and cofactor binding pockets in nucleic acids pre-catalysts. Catalytic quadruplexes (G4s) offer a unique opportunity to tackle this issue, thanks to external G-quartets that constitute more defined catalytic centers. When combined with hemin, G4/hemin systems behave as hemoproteins (*e.g.*, peroxidases) capable of performing H_2O_2-promoted catalytic oxidations. A great deal of research has been devoted to improve the performances of catalytic G4s, with a particular focus on their sequences (that govern their topology and stability) and the hemin-binding sites (the external G-quartet and surrounding nucleobases). Here, we report on a new strategy implemented to increase the catalytic potential of G4s *via* a modification of their inner backbones (5′-5′ inversion of polarity site in the middle of the G4-forming DNA strands). This chemical modification uniquely allows for obtaining G4s with two identical external G-quartets, i.e., two 3′-ends, known to be critical for hemin binding and catalysis. In light of literature precedents, we also introduced dA caps on top of the 3′-ends, given that these additional nucleobases actively participate to hemin fixation and activation. Our optimal G4 systems AG_2-G_2A and AG_3-G_3A were shown to display far better catalytic performances (in the model ABTS oxidation reaction) than their unmodified counterparts AG_4A and AG_6A, thereby lending credence to the relevance of our strategy. We also showed that their thermal stability allows for being used as thermophilic DNAzymes, further increasing the interest and scope of this new class of catalytic G4s. These results thus add another string to the bow of chemical modifications that make G4 pre-catalysts still more effective. More examples of G4s with 5′-5′ inversion of polarity site will be soon developed to bring catalytic G4s ever closer to the performances of related hemoproteins.

Acknowledgments

This work was financially supported by the Department of Pharmacy, University of Naples Federico II, Fondo di finanziamento per le attività base di ricerca (FFABR 2017) for V.E. and A.V., the CNRS (D.M.) and the Agence Nationale de la Recherche (ANR-17-CE17-0010-01 for P.L. and D.M.). This project is part of the project "Pharmaco-imagerie & agents théranostiques" supported by the Université de Bourgogne and Conseil Régional de Bourgogne (PARI) and the European Union (PO FEDER-FSE Bourgogne 2014/2020 programs).

There are no conflicts of interest to declare.

Appendix A. Supplementary material

Supplementary data to this article can be found online at https://doi.org/10.1016/j.ijbiomac.2019.10.181.

References

[1] D. Sen, L.C.H. Poon, RNA and DNA complexes with hemin [Fe(III) heme] are efficient peroxidases and peroxygenases: how do they do it and what does it mean? Crit. Rev. Biochem. Mol. Biol. 46 (2011) 478–492, https://doi.org/10.3109/10409238.2011.618220.
[2] Y. Li, D. Sen, A catalytic DNA for porphyrin metallation, Nat. Struct. Biol. 3 (1996) 743–747, https://doi.org/10.1038/nsb0996-743.
[3] P. Travascio, Y. Li, D. Sen, DNA-enhanced peroxidase activity of a DNA aptamer-hemin complex, Chem. Biol. 5 (1998) 505–517, https://doi.org/10.1016/S1074-5521(98)90006-0.
[4] P. Travascio, P.K. Witting, A.G. Mauk, D. Sen, The peroxidase activity of a hemin-DNA oligonucleotide complex: free radical damage to specific guanine bases of the DNA, J. Am. Chem. Soc. 123 (2001) 1337–1348, https://doi.org/10.1021/ja0023534.
[5] L. Stefan, F. Denat, D. Monchaud, Insights into how nucleotide supplements enhance the peroxidase-mimicking DNAzyme activity of the G-quadruplex/hemin system, Nucleic Acids Res. 40 (2012) 8759–8772, https://doi.org/10.1093/nar/gks581.
[6] H. Shimizu, H. Tai, K. Saito, T. Shibata, M. Kinoshita, Y. Yamamoto, Characterization of the Interaction between Heme and a Parallel G-Quadruplex DNA Formed from d(TTAGGGT), Bull. Chem. Soc. Jpn. 88 (2015) 644–652, https://doi.org/10.1246/bcsj.20140374.
[7] J. Chen, Y. Zhang, M. Cheng, Y. Guo, J. Šponer, D. Monchaud, J.L. Mergny, H. Ju, J. Zhou, How proximal nucleobases regulate the catalytic activity of G-quadruplex/hemin DNAzymes, ACS Catal. 8 (2018) 11352–11361, https://doi.org/10.1021/acscatal.8b03811.
[8] K. Saito, H. Tai, H. Hemmi, N. Kobayashi, Y. Yamamoto, Interaction between the heme and a G-quartet in a heme-DNA complex, Inorg. Chem. 51 (2012) 8168–8176, https://doi.org/10.1021/ic3005739.
[9] J.L. Mergny, D. Sen, DNA quadruple helices in nanotechnology, Chem. Rev. 119 (2019) 6290–6325, https://doi.org/10.1021/acs.chemrev.8b00629.
[10] B.T. Roembke, S. Nakayama, H.O. Sintim, Nucleic acid detection using G-quadruplex amplification methodologies, Methods. 64 (2013) 185–198, https://doi.org/10.1016/j.ymeth.2013.10.003.
[11] F. Wang, C.H. Lu, I. Willner, From cascaded catalytic nucleic acids to enzyme-DNA nanostructures: controlling reactivity, sensing, logic operations, and assembly of

complex structures, Chem. Rev. 114 (2014) 2881–2941, https://doi.org/10.1021/cr400354z.
[12] Z. Hu, Z. Suo, W. Liu, B. Zhao, F. Xing, Y. Zhang, L. Feng, DNA conformational polymorphism for biosensing applications, Biosens. Bioelectron. 131 (2019) 237–249, https://doi.org/10.1016/j.bios.2019.02.019.
[13] L. Gong, Z. Zhao, Y.F. Lv, S.Y. Huan, T. Fu, X.B. Zhang, G.L. Shen, R.Q. Yu, DNAzyme-based biosensors and nanodevices, Chem. Commun. 51 (2015) 979–995, https://doi.org/10.1039/c4cc06855f.
[14] J. Kosman, B. Juskowiak, Peroxidase-mimicking DNAzymes for biosensing applications: a review, Anal. Chim. Acta. 707 (2011) 7–17, https://doi.org/10.1016/j.aca.2011.08.050.
[15] W. Zhou, R. Saran, J. Liu, Metal Sensing by DNA, Chem. Rev. 117 (2017) 8272–8325, https://doi.org/10.1021/acs.chemrev.7b00063.
[16] M.R. Saidur, A.R.A. Aziz, W.J. Basirun, Recent advances in DNA-based electrochemical biosensors for heavy metal ion detection: a review, Biosens. Bioelectron. 90 (2017) 125–139, https://doi.org/10.1016/j.bios.2016.11.039.
[17] S. Zhan, Y. Wu, L. Wang, X. Zhan, P. Zhou, A mini-review on functional nucleic acids-based heavy metal ion detection, Biosens. Bioelectron. 86 (2016) 353–368, https://doi.org/10.1016/j.bios.2016.06.075.
[18] D.L. Ma, D.S.H. Chan, B.Y.W. Man, C.H. Leung, Oligonucleotide-based luminescent detection of metal ions, Chem. – An Asian J. 6 (2011) 986–1003, https://doi.org/10.1002/asia.201000870.
[19] T. Kilic, A. Erdem, M. Ozsoz, S. Carrara, microRNA biosensors: opportunities and challenges among conventional and commercially available techniques, Biosens. Bioelectron. 99 (2018) 525–546, https://doi.org/10.1016/j.bios.2017.08.007.
[20] M. Mahdiannasser, Z. Karami, An innovative paradigm of methods in microRNAs detection: highlighting DNAzymes, the illuminators, Biosens. Bioelectron. 107 (2018) 123–144, https://doi.org/10.1016/j.bios.2018.02.020.
[21] D.M. Kong, Factors influencing the performance of G-quadruplex DNAzyme-based sensors, Methods 64 (2013) 199–204, https://doi.org/10.1016/j.ymeth.2013.07.013.
[22] L. Zhu, C. Li, Z. Zhu, D. Liu, Y. Zou, C. Wang, H. Fu, C.J. Yang, In vitro selection of highly efficient G-quadruplex-based DNAzymes, Anal. Chem. 84 (2012) 8383–8390, https://doi.org/10.1021/ac301899h.
[23] J. Chen, Y. Guo, J. Zhou, H. Ju, The Effect of Adenine Repeats on G-quadruplex/hemin Peroxidase Mimicking DNAzyme Activity, Chem. – A Eur. J. 23 (2017) 4210–4215, https://doi.org/10.1002/chem.201700040.
[24] W. Li, Y. Li, Z. Liu, B. Lin, H. Yi, F. Xu, Z. Nie, S. Yao, Insight into G-quadruplex-hemin DNAzyme/RNAzyme: adjacent adenine as the intramolecular species for remarkable enhancement of enzymatic activity, Nucleic Acids Res. 44 (2016) 7373–7384, https://doi.org/10.1093/nar/gkw634.
[25] T. Chang, H. Gong, P. Ding, X. Liu, W. Li, T. Bing, Z. Cao, D. Shangguan, Activity Enhancement of G-Quadruplex/Hemin DNAzyme by Flanking d(CCC), Chem. – A Eur. J. 22 (2016) 4015–4021, https://doi.org/10.1002/chem.201504797.
[26] D.M. Kong, J. Xu, H.X. Shen, Positive effects of ATP on G-quadruplex-hemin DNAzyme-mediated reactions, Anal. Chem. 82 (2010) 6148–6153, https://doi.org/10.1021/ac100940v.
[27] L. Stefan, F. Denat, D. Monchaud, Deciphering the DNAzyme activity of multimeric quadruplexes: Insights into their actual role in the telomerase activity evaluation assay, J. Am. Chem. Soc. 133 (2011) 20405–20415, https://doi.org/10.1021/ja208145d.
[28] C. Qi, N. Zhang, J. Yan, X. Liu, T. Bing, H. Mei, D. Shangguan, Activity enhancement of G-quadruplex/hemin DNAzyme by spermine, RSC Adv. 4 (2014) 1441–1448, https://doi.org/10.1039/c3ra45429k.
[29] E. Golub, H.B. Albada, W.C. Liao, Y. Biniuri, I. Willner, Nucleoapzymes: Hemin/G-quadruplex DNAzyme-aptamer binding site conjugates with superior enzyme-like catalytic functions, J. Am. Chem. Soc. 138 (2016) 164–172, https://doi.org/10.1021/jacs.5b09457.
[30] Y. Guo, J. Chen, M. Cheng, D. Monchaud, J. Zhou, H. Ju, A Thermophilic Tetramolecular G-Quadruplex/Hemin DNAzyme, Angew. Chemie - Int. Ed. 56 (2017) 16636–16640, https://doi.org/10.1002/anie.201708964.
[31] V. Esposito, A. Virgilio, A. Randazzo, A. Galeone, L. Mayol, A new class of DNA quadruplexes formed by oligodeoxyribonucleotides containing a 3'-3' or 5'-5' inversion of polarity site, Chem. Commun. (Camb). (2005) 3953–3955, https://doi.org/10.1039/b504455c.
[32] V. Esposito, A. Virgilio, A. Pepe, G. Oliviero, L. Mayol, A. Galeone, Effects of the introduction of inversion of polarity sites in the quadruplex forming oligonucleotide TGGGT, Bioorganic Med. Chem. 17 (2009) 1997–2001, https://doi.org/10.1016/j.bmc.2009.01.027.
[33] J. Kypr, I. Kejnovská, D. Renčiuk, M. Vorlíčková, Circular dichroism and conformational polymorphism of DNA, Nucleic Acids Res. 37 (2009) 1713–1725, https://doi.org/10.1093/nar/gkp026.
[34] S. Masiero, R. Trotta, S. Pieraccini, S. De Tito, R. Perone, A. Randazzo, G.P. Spada, A non-empirical chromophoric interpretation of CD spectra of DNA G-quadruplex structures, Org. Biomol. Chem. 8 (2010) 2683–2692, https://doi.org/10.1039/c003428b.
[35] L. Stefan, D. Duret, N. Spinelli, E. Defrancq, D. Monchaud, Closer to nature: An ATP-driven bioinspired catalytic oxidation process, Chem. Commun. 49 (2013) 1500–1502, https://doi.org/10.1039/c2cc38317a.
[36] J. Liu, Z. Cao, Y. Lu, Functional nucleic acid sensors, Chem. Rev. 109 (2009) 1948–1998, https://doi.org/10.1021/cr030183i.